

The stability of aluminum-manganese intermetallic phases under the microgalvanic coupling conditions anticipated in magnesium alloys

R. M. Asmussen, W. J. Binns, R. Partovi-Nia, P. Jakupi and D. W. Shoesmith*

The electrochemical behaviour of two Al-Mn materials (Al- 5.5 at % Mn and Al-13.5 at % Mn) has been studied in 0.275 M NaCl and 0.138 M MgCl₂ solutions to simulate the cathodic environment of Al-Mn particles during the corrosion of a Mg alloy. Upon polarization in NaCl solution to a potential in the range expected on a corroding Mg alloy, the Al-5.5 at % Mn alloy proved unstable undergoing de-alloying (loss of Al) and delamination of layers of the Al(OH)₃ formed. This leads to a steady increase H₂O reduction current. When polarized in MgCl₂ solution the surface was partially protected from de-alloying and the current for H₂O reduction suppressed by the deposition of Mg(OH)₂. The Al-13.5 at % Mn alloy was considerably more stable when cathodically polarized. This increased stability was attributed to the higher density of Mn-enriched areas in the alloy surface. This simulation of the microgalvanic cathodic behaviour of Al-Mn intermetallic particles confirms that the appearance of corrosion product domes on the Al-Mn intermetallic particles during the corrosion of Mg alloys as an indication of their cathodic behaviour and that Al-Mn intermetallic particles are efficient, yet unstable cathodes.

1 Introduction

Lightweight Mg alloys have promising applications in the automotive and aerospace fields due to their high strength to weight ratio [1], but experience rapid corrosion when coupled to a more noble material [2]. Impurities found in Mg alloys such as Fe and Cu [3–5] are detrimental to the corrosion properties of the alloy. However, their distribution can be limited through the addition of Mn which can scavenge these elements in the melt leading to improved corrosion performance [6–8]. However, the formation of Al-Mn intermetallic particles can render the α -Mg matrix susceptible to microgalvanic corrosion. It is generally accepted that such particles, especially when contaminated with Fe [9], can act as cathodes in a range of Mg alloys [10]. Microgalvanic coupling of Al₂Mn particles in the AZ31, AZ80 and AZ91D alloys was shown to cause localized corrosion in the vicinity of the particles [11] in 3.5 wt% NaCl. In salt fog experiments AlMn particles ranging in composition from Al₁₉Mn₄ (Al_{4.75}Mn) to Al₈Mn₅ (Al_{1.6}Mn) only influenced the early stages of alloy corrosion but no explanation for this short

term activity was noted [12]. Studies using custom synthesized AlMn specimens with a high Mn content (Al_{1.5}Mn) showed only very weak galvanic activity when coupled to the AZ91 alloy [13]. However, these last experiments were conducted in low ionic strength solutions containing only millimolar concentrations of Na₂SO₄ and NaCl in which the range of microgalvanic couples would be limited.

On corroded Mg alloys, some Al-Mn intermetallic particles have been observed to collect a dome of deposited corrosion product [11,14] while others remain exposed, a trait also observed on supposed cathodic sites on other Mg alloys [15–17]. Based on scanning electrochemical microscopy (SECM) measurements, it was suggested that deposition of corrosion products occurred on cathodically active sites [18,19] with microscopic evidence of corrosion product accumulation [19] at these sites. Recently, we suggested that these corrosion product deposits on Al-Mn intermetallic particles (Al₈Mn₅ (Al_{1.6}Mn)) in the AM50 alloy are a result of their cathodic behaviour when microgalvanically-coupled to the α -Mg matrix²⁰, with the cathodic reaction being the reduction of H₂O to H₂ [8]. As H₂ production proceeds, the local pH at the cathode surface increases leading to two observable features: (i) deposition of Mg(OH)₂ to create the corrosion product dome; and (ii) delamination of the surface of the intermetallic due to the loss by dissolution of Al [20]. These results suggest that the activity of these intermetallic phases may

R. M. Asmussen, W. J. Binns, R. Partovi-Nia, P. Jakupi, D. W. Shoesmith
Department of Chemistry and Surface Science Western, Western
University, 1151 Richmond St, London, Ontario, Canada
E-mail: dwshoesm@uwo.ca

be limited by this combination of deposition and metallic instability.

The cathodic performance of many of the commonly encountered intermetallic phases in Al and Mg alloys has been assessed [21–23] using potentiodynamic polarization measurements and, in the case of Al alloys, their cathodic performance evaluated when polarized to the corrosion potential that would be established on exposing the Al alloy (~ -900 mV vs. SCE to -965 mV vs. SCE) [21,24]. The Al_6Mn intermetallic phase was found to be a relatively active cathode. While these measurements provide a guide to which phases are likely to act as the dominant cathodes in microgalvanic corrosion processes they do not define their overall reactivity which will be controlled by features such as their composition, location within the matrix and the ionic strength of the exposure environment. Additionally the deposition of corrosion products and their stability/instability in the local chemical environments generated as corrosion progresses could substantially alter their cathodic reactivity.

In this study we have attempted to study the cathodic behaviour of Al-Mn intermetallic particles using bulk Al-Mn electrodes using the cathodic polarization technique employed previously for the secondary phases anticipated in Al alloys [21,24]. The primary goals were (i) to determine how their cathodic reactivity changed as corrosion progressed and their composition, physical structure and surface properties changed; (ii) to demonstrate the delamination and dissolution of Al observed on Al_8Mn_5 intermetallic particles as a consequence of their cathodic activity [20]; and (iii) to confirm that the rapid accumulation of a dome of corrosion products on particles in a Mg alloy is an indication of the cathodic activity of the consequently disguised microstructural feature.

2 Experimental

2.1 Materials

Mg alloy AZ31 (O-temper) was provided as a rolled sheet, 1 mm in thickness, by General Motors (Canada). Samples were machined into $1\text{ cm} \times 1\text{ cm} \times 1\text{ mm}$ electrodes, and ground successively with 800, 1000, 1200, 2400 grit SiC, and then polished using a $3\text{ }\mu\text{m}$ diamond suspension with ethanol-isopropanol as the lubricant. A final polish was achieved using $0.4\text{ }\mu\text{m}$ colloidal silica with ethylene glycol as a lubricant. Following polishing, the sample was rinsed in ethanol and dried in a stream of ultra-high purity Ar.

Two Al-Mn materials, supplied by CANMET Materials (Hamilton, ON, Canada), were used in this study; Al-5.5 at % Mn (Al-5.5Mn) and Al-13.5 at % Mn (Al-13.5Mn). The samples were machined into $1\text{ cm} \times 1\text{ cm} \times 0.7\text{ cm}$ pieces and one face threaded to allow electrical connection to external circuitry. All samples were mounted in Struers EpoFix[®] epoxy resin to limit electrolyte exposure to solution to a single face of the intermetallic. Prior to each experiment the samples were ground successively with 800, 1000, 1200, 2400 and 4000 grit SiC paper using water as a lubricant. Solutions were prepared using reagent grade NaCl and $\text{MgCl}_2 \cdot 6\text{H}_2\text{O}$ (99% assay, Caledon) and NanoPure[®] water ($18\text{ M}\Omega \cdot \text{cm}$).

2.2 Electrochemical measurements

Electrochemical experiments on the Al-Mn electrodes were performed in a standard three-electrode electrochemical cell equipped with a Pt-foil counter electrode and a saturated calomel reference electrode (SCE). All experiments were performed in naturally aerated NaCl or MgCl_2 (both reagent grade, 99% assay) solutions prepared with MilliQ water ($18\text{ M}\Omega \cdot \text{cm}$) at ambient temperature ($\sim 22\text{ }^\circ\text{C}$). In immersion experiments, AZ31 and the Al-Mn specimens were exposed face down in the solution, suspended by a steel rod. Electrochemical control was provided by a Solartron[®] 1480 MultiStat. In cathodic potentiodynamic polarization (PDP) measurements, the Al-Mn electrodes were exposed to solution for 1 h to 3 h to establish a stable corrosion potential (E_{CORR}), and then polarized at a rate of 1 mV/s from E_{CORR} to -1.55 V vs. SCE, and held for 20 h.

2.3 Surface analysis

Stereo-micrographs of the Al-Mn specimens were collected on a Zeiss SteReo Lumar V12 Microscope equipped with an Axio 1.0 camera. Scanning electron microscopy (SEM) and energy dispersive X-ray spectroscopy (XEDS) were performed on either a Hitachi 3400-N Variable Pressure scanning electron microscope, a LEO 440 scanning electron microscope equipped with a Quartz One XEDS detector, or a LEO (Zeiss) 1540 XB/SEM equipped with an Oxford instruments EDX detector. Cross-sections were formed with a focused ion beam (FIB) on a LEO 1540 XB/SEM using a Ga ion beam. X-ray diffraction (XRD) was carried out using a Bruker D8 fully automated diffractometer employing Co $K\alpha$ radiation ($\lambda = 1.78897\text{ \AA}$) and peak identification was confirmed with X-Pert High Score Plus software.

3 Results

3.1 Behaviour of Al-Mn intermetallic particles

An example of the size and distribution of Al-Mn intermetallic particles on a polished AZ31 Mg alloy is shown in Figure 1(a). The large particle marked with a white arrow is magnified in Figure 1(b). The contrast observed within the intermetallic is due to the presence of segregated regions with different Al:Mn ratios, confirmed by XEDS analyses, Figure 1(c), of the two sites marked in Figure 1(b). The quantitative XEDS data (in at %) is presented in Table 1. Site 1 has an Al:Mn ratio of 11:4, and Site 2 of 8:5, indicating the regions to be $\text{Al}_{11}\text{Mn}_4$ ($\text{Al}_{2.75}\text{Mn}$) and Al_8Mn_5 ($\text{Al}_{1.6}\text{Mn}$), respectively. Regions with different amounts of Al and Mn are to be expected based on the Al-Mn phase diagram and on studies which show multiple compositions of Al-Mn intermetallics in Mg alloys ranging from Al_9Mn_4 to Al_8Mn_5 [12,25]. Following exposure of the AZ31 alloy to 0.275 M NaCl for 24 h, domes of corrosion product were observed above Al-Mn intermetallic particles as shown in Figure 1(d), for the line of particles marked with a red arrow in Figure 1(a). In our previous study on the AM50 Mg alloy [20] the accumulation of such a

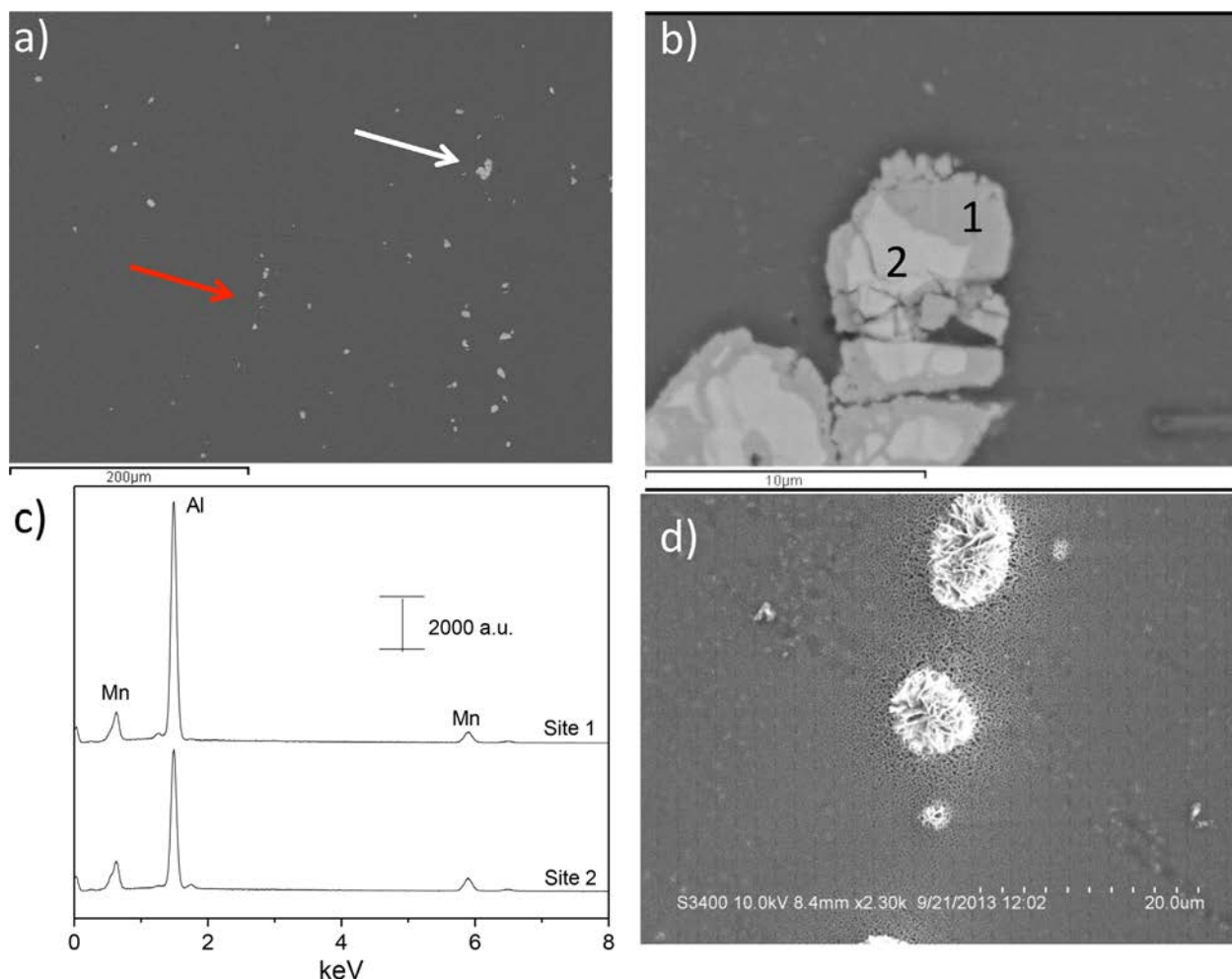


Figure 1. a) SEM micrograph of a polished AZ31 Mg alloy surface, b) SEM micrograph of the Al-Mn intermetallic marked with the white arrow in (a), c) XEDS spectra of the locations marked in (b), d) SEM micrograph of the domes of corrosion product that appeared above the Al-Mn intermetallic particles marked with the red arrow in (a) following 24 h immersion in 0.275 M NaCl.

corrosion product dome was interpreted to indicate that the intermetallic functioned as a cathode galvanically coupled to the corroding α -Mg matrix, a similar interpretation can be made for the AZ31 alloy.

Figure 2(a-I) shows a backscatter SEM micrograph of the surface of the Al-5.5Mn specimen. The darker areas of the surface were higher in Al content, confirmed by the XEDS map in Figure 2(a-II), whereas the brighter areas were rich in Mn, Figure 2(a-IV). The Mn-rich regions had a Mn content ranging from 11 at % to 20 at %, with an average of 15 at %, indicating a composition close to

Table 1. Quantitative XEDS data, in at %, of the major elements from the corresponding spectra in Figure 1 (c).

Element (at%)	Site 1	Site 2
Mg	1.4	0.6
Al	71.6	62.0
Mn	27.0	37.4
Zn	0	0

Al_6Mn , although regions with a higher Mn content (~ 20 at %), seen as the lightest coloured regions in the image, may be Al_4Mn . Little Mn was present outside these locations, only 3-5 at % Mn being detected in the Al-rich regions. Many small locations containing Si were also present, Figure 2(a-III). A similar set of images and analyses shows the Al-13.5Mn specimen, Figure 2(b), had a more dendritic appearance with 11 at % to 18 at % Mn in the lighter regions, Figure 2(b-IV), indicating a similar composition to that observed in the Mn-rich regions in Al-5.5Mn. Although not immediately clear in Figure 2(b-1) the Al-5.5Mn exhibits a cross banded interlacing of the Mn-rich phase(s). These analyses show that both alloys are composed of two phases; a phase in the composition range Al_6Mn to Al_4Mn and a second phase containing only 3 to 5 at % Mn. The primary difference between the alloys is the density of Mn-rich regions being considerably higher for Al-13.5Mn. This last specimen also has a smaller number of Si-containing locations, Figure 2(b-III). Comparison of the XEDS maps for both specimens shows the Si-rich particles are associated with the Al-rich regions of both alloys, although Si is known to be inert in the corrosion of Mg alloys [26].

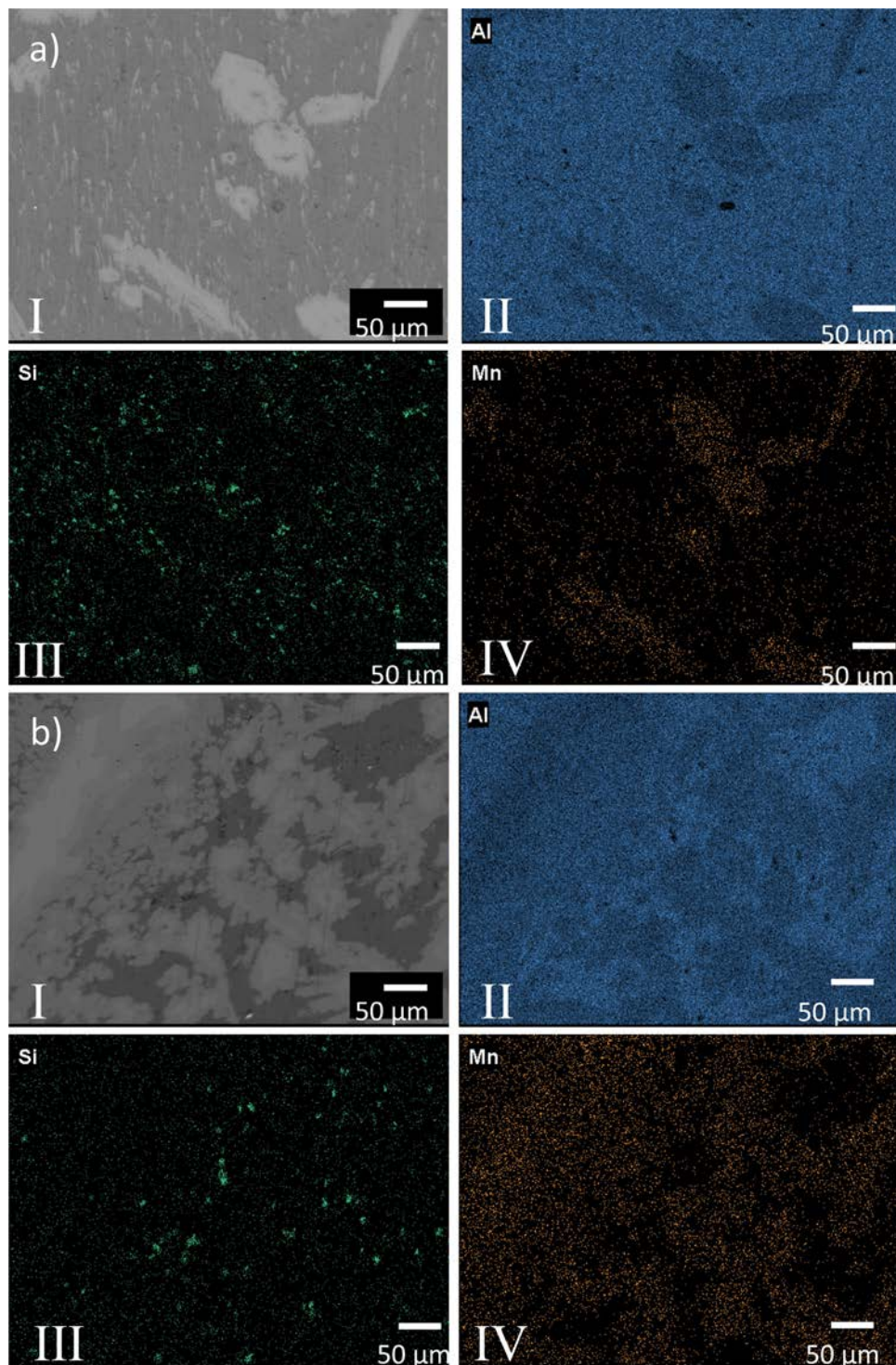


Figure 2. I) SEM backscatter micrograph of the a) Al-5.5Mn and b) Al-13.5Mn surface following polishing and the corresponding XEDS maps for II) Al, III) Si and IV) Mn.

3.2 Electrochemical behaviour

Electrochemical measurements were performed on both alloys in either 0.275 M NaCl or 0.138 M MgCl₂; i.e., solutions with a similar Cl⁻ concentration but containing different cations. The Mg²⁺ solution was chosen to simulate the supply of

Mg²⁺ anticipated from adjacent corroding α-Mg locations when Al-Mn intermetallic particles are galvanically-coupled within a Mg alloy. A concentration of 0.138 M was chosen since it is within the range of the measured Mg²⁺ concentration above a galvanically coupled corroding Mg sample measured using SECM with a potentiometric sensor [27,28].

Figure 3 shows the E_{CORR} measured on both Al-5.5Mn and Al-13.5Mn over ~ 12 h immersion periods in these solutions, with Al-5.5Mn exhibiting more positive E_{CORR} values than Al-13.5Mn in both solutions. This may reflect the slightly greater passive nobility of the specimen containing the larger coverage of Al-rich regions. Magnification of the negative-going potential transients observed on Al-5.5Mn in the NaCl solution shows they are of the form expected for metastable pitting events. Examination of the surface shows these are dominantly associated with the Al-rich regions and the boundaries between the two phases within the Mn-rich areas. The cathodic PDP curves are plotted in Figure 4. Consistent with the results in Figure 3, Al-5.5Mn again exhibited a more positive E_{CORR} than Al-13.5Mn. On scanning from E_{CORR} to -1.55 V both materials displayed similar currents in the MgCl_2 solution for potentials < -1.0 V. In 0.275 M NaCl, slightly larger currents were observed especially for Al-5.5Mn which exhibited a sharp increase in current at potentials < -1.1 V. At -1.55 V, the electrodes all showed currents in the region of $-100 \mu\text{A} \cdot \text{cm}^{-2}$.

To determine their potential cathodic activity, the electrodes were polarized at -1.55 V for 20 h: i.e., in the potential range where Al-Mn intermetallic particles would be polarized if acting as microgalvanically-coupled cathodes in a corroding Mg alloy [29]. The currents recorded are shown in Figure 5. In the MgCl_2 solution the cathodic current on both alloys rapidly decreased to steady state values of $-100 \mu\text{A} \cdot \text{cm}^{-2}$ (Al-5.5Mn) and $-40 \mu\text{A} \cdot \text{cm}^{-2}$ (Al-13.5Mn); i.e., to values similar to those measured in the PDP scans, Figure 4. In NaCl, the cathodic current recorded on Al-13.5Mn showed a similar decrease to a steady value of $-20 \mu\text{A} \cdot \text{cm}^{-2}$ after ~ 1 h of polarization. However, after a similar initial decrease, the cathodic current recorded on Al-5.5Mn in NaCl steadily increased to a final value of $-800 \mu\text{A} \cdot \text{cm}^{-2}$. Over the 20 h period, the cathodic current exhibited a number of ill-defined peaks before suddenly increasing again. A particularly large such transient was observed between 11 and 13 h. The reproducibility of this behaviour on Al-5.5Mn in NaCl is demonstrated in the inset in Figure 5.

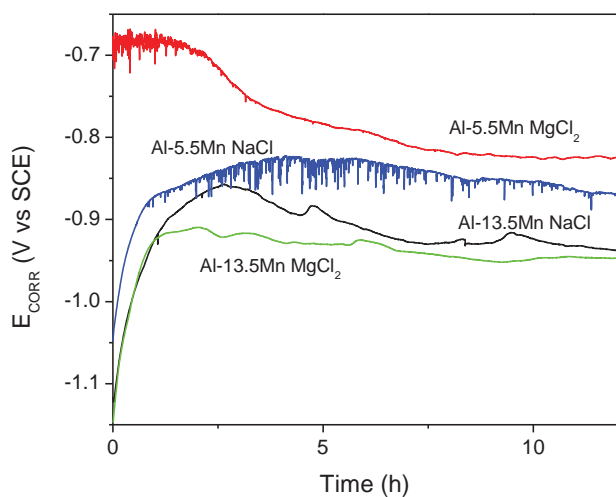


Figure 3. Evolution of E_{CORR} over a 12 h period of immersion in 0.275 M NaCl and 0.138 M MgCl_2 for the Al-5.5Mn and Al-13.5Mn electrodes.

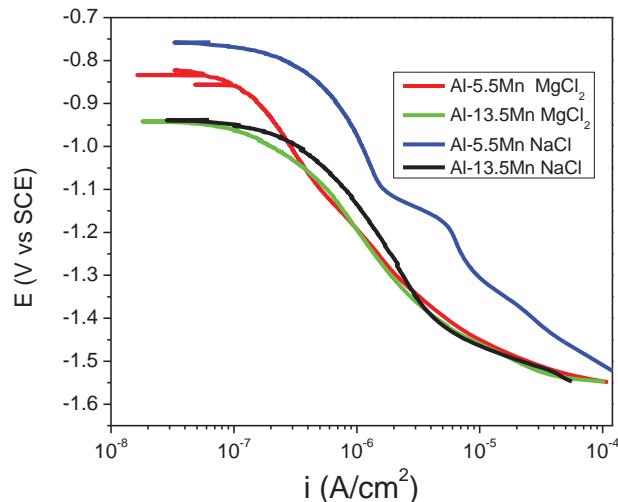


Figure 4. PDP scans recorded on the Al-5.5Mn and Al-13.5Mn electrodes in 0.275 M NaCl and 0.138 M MgCl_2 from E_{CORR} to -1.55 V at a scan rate of 1 mV/s.

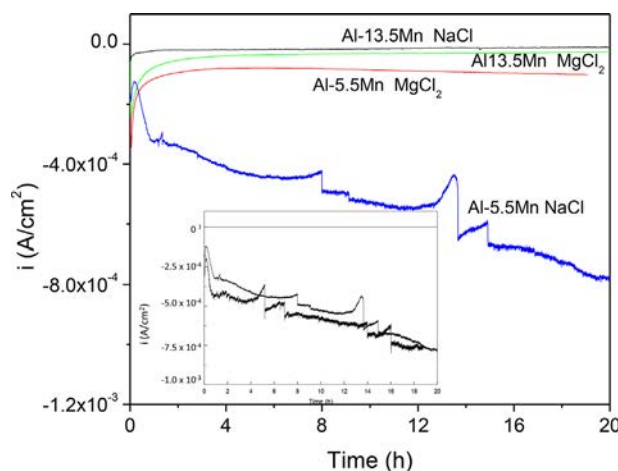


Figure 5. Potentiostatic current density vs. time profiles recorded on the Al-5.5Mn and Al-13.5Mn electrodes at -1.55 V in 0.138 M MgCl_2 and 0.275 M NaCl. Inset shows the reproducibility of the behaviour seen on Al-5.5Mn in 0.275 M NaCl.

3.3 Surface behaviour

Following both corrosion and electrochemical experiments, the surfaces of the Al-5.5Mn specimens were investigated optically and by SEM. After 12 h of immersion at E_{CORR} in either NaCl or MgCl_2 neither electrode exhibited any surface deposits. The absence of any significant corrosion was confirmed by their retention of a metallic luster as shown for Al-5.5Mn in Figures 6 (a) and 6(b). After potentiostatic polarization to -1.55 V for 20 h obvious changes to the surface of the Al-5.5Mn electrode were observed. In NaCl, the surface was distinctly discoloured, Figure 6(c), indicating significant degradation, and in MgCl_2 a dense white deposit had accumulated, Figure 6(d). For the Al-13.5Mn alloy the changes to the surface were not so obvious in optical micrographs (not shown).

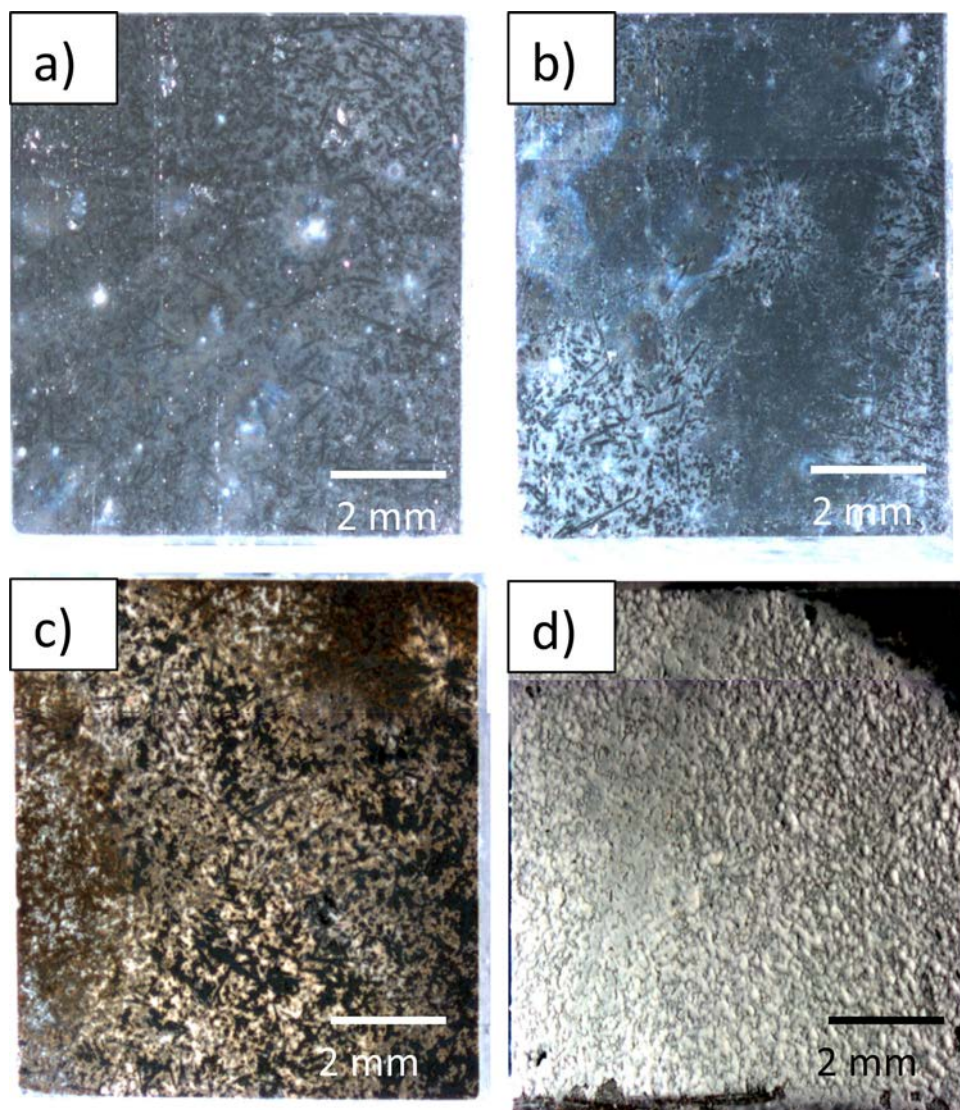


Figure 6. Optical micrographs of the Al-5.5Mn surface following a 20 h exposure to a) 0.275 M NaCl at E_{CORR} , b) 0.138 M MgCl_2 at E_{CORR} , c) 0.275 M NaCl at -1.55 V, and d) 0.138 M MgCl_2 at -1.55 V.

The changes on the surface of the Al-5.5Mn electrode after the potentiostatic treatment in NaCl were clearly visible by SEM, Figure 7(a). Two distinct regions were observed, a dark grey region corresponding to the Al-rich phase seen in Figure 2(a) and lighter bands corresponding to the Mn-rich phase, also seen in Figure 2. At an increased magnification, Figure 7(b), the dark grey (Al) regions were observed to be covered with columnar crystals, as seen on the left and right sides of the image, while other areas were free of such crystals and covered with a finer deposit. The XEDS analyses of these regions, recorded at Sites 1 and 2 (Figure 7(b)), Figure 7(c), showed the crystal-covered area (Site 1) contained Al and O, whereas the crystal-free area (Site 2) was lower in Al with an observable amount of Mn. The Al-13.5Mn electrode also showed the same distinct behavior on the Al-rich and Mn-rich areas of the surface, Figure 7(d), although the extent of reaction was lower.

For the Al-5.5Mn electrode a FIB cross section was cut across the edge between Sites 1 and 2 in Figure 7(b) to reveal the

underlying surface and the morphology of the surface layer, Figure 8(a). XEDS analyses of the numbered sites are shown in Figure 8(b). Site 1 is an Al-rich region, the absence of an O signal confirming that this is the substrate. Site 2 corresponds to a Mn rich region, the small O signal suggesting a thin oxide may be present on the bottom surface of the major fracture just above the site. Sites 3 and 4 are Al oxide (hydroxide). The absence of a Mn signal at these locations suggests it is not the corrosion product from the Mn-rich region below it (Site 2). The thickness of the corrosion product at this location is $\sim 8 \mu\text{m}$ to $10 \mu\text{m}$ with an extensively damaged region immediately below it. The most likely scenario is that this is the corrosion product from a completely destroyed Al-rich region. This claim is supported by the composition of Site 5 which is an Mn-rich oxide containing a significant amount of Al; suggesting it is the corrosion product formed on an Mn-rich area of the surface. The corrosion product layer at this location is only $\sim 3 \mu\text{m}$ to $4 \mu\text{m}$ thick and there is very little damage to the region immediately below this site. The

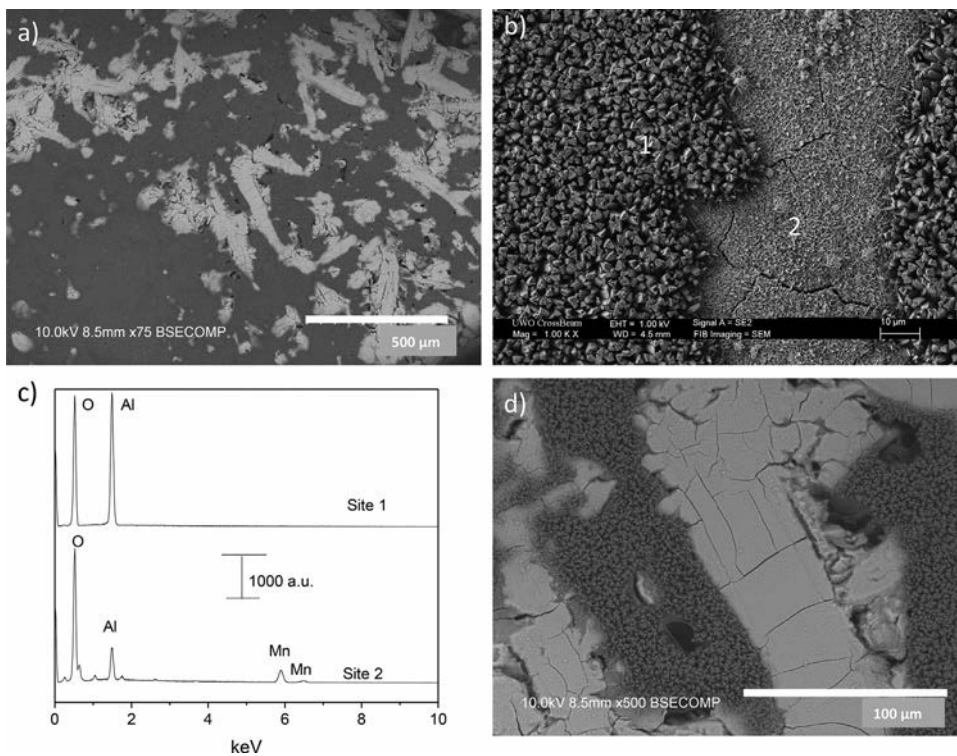


Figure 7. SEM micrograph of the surface of the Al-5.5Mn electrode at a) 75 x magnification and b) 1000x magnification and c) the corresponding XEDS spectra recorded after 20 h cathodic polarization at -1.55 V in 0.275 M NaCl. The location of the bulky crystals in Site 1 and of the small layer in Site 2 are labelled with the arrow in (a), d) SEM micrograph of the Al-13.5Mn electrode following 20 h cathodic polarization at -1.55 V in 0.275 M NaCl.

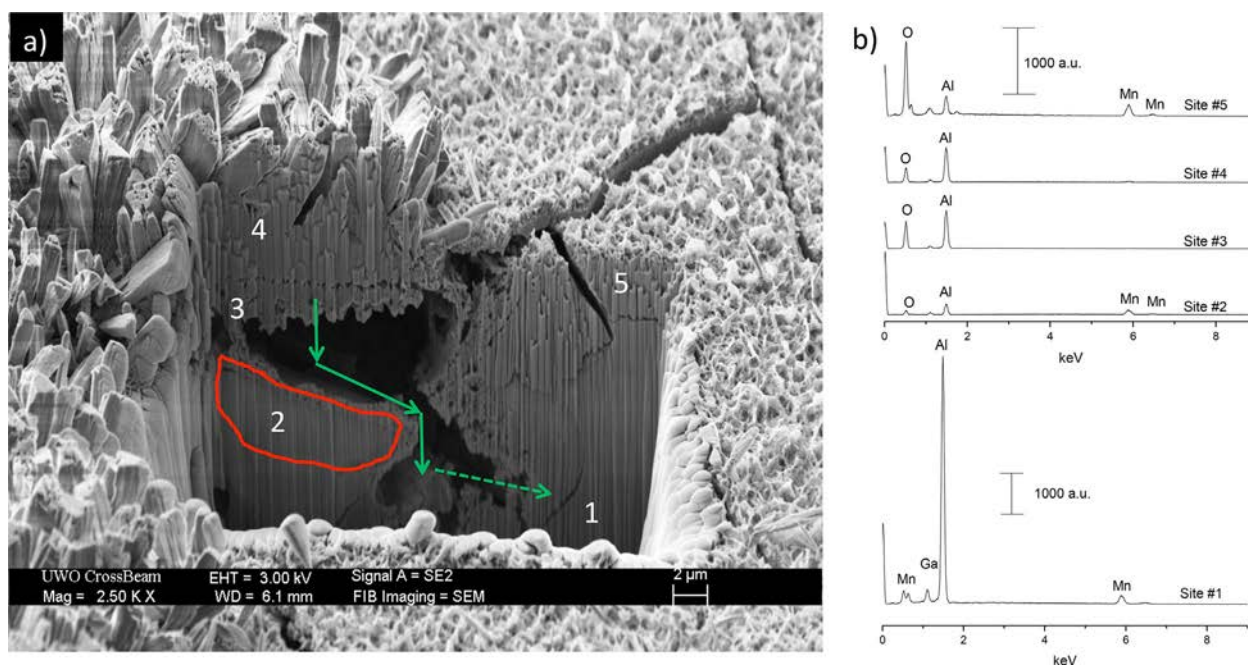


Figure 8. a) SEM image of a FIB on the Al-5.5Mn electrode after cathodic polarization at -1.55 V in 0.275 M NaCl. A Mn-rich region lying below the initial surface, Site 2, is outlined in red, and the progression of corrosion moving away from this region is marked with the green arrows and b) corresponding XEDS spectra for the sites indicated in (a).

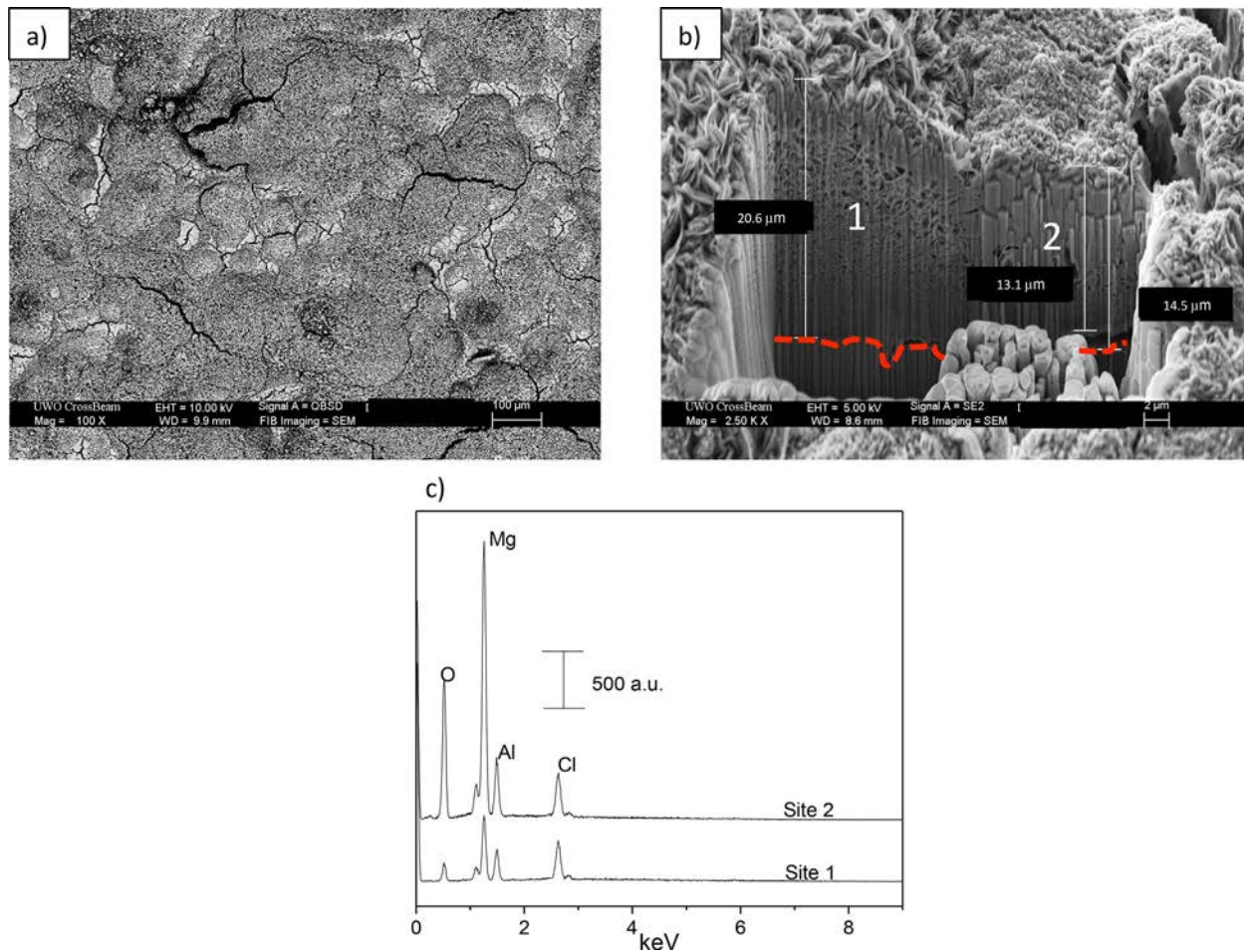


Figure 9. a) SEM micrograph of the Al-5.5Mn surface following cathodic polarization for 20 h at -1.55 V in 0.138 M MgCl_2 , b) FIB cross section through the surface layer with the red dotted line denoting the substrate/layer interface and c) XEDS spectra recorded at the sites labelled in (b).

area just below Site 5 contained 11.1 % Mn indicating it was an Mn-rich region.

The surface of this electrode (Al-5.5Mn) after potentiostatic polarization at -1.55 V in the MgCl_2 solution showed a much different morphology, the surface being covered with a compact, generally uniform deposit, Figure 9(a). The cracking observed most likely occurred on drying the surface after removal from the cell. A FIB cross section of the surface, Figure 9 (b), revealed a much thicker deposited layer of $\sim 20 \mu\text{m}$ compared to that formed in the NaCl solution. XEDS analyses, Figure 9(c), showed the layer at Site 1 was a mainly Mg-containing oxide/hydroxide with a small, but significant, Al content. Analysis of Site 2 yielded much stronger Mg and O signals compared to Al. The overall increase in signal strength compared to Site 1 was likely a result of the lower porosity of the layer at Site 2, Figure 9(b). The interface between the substrate and the deposit is indicated by the red line. The substrate at this location had a 2 at% Mn content confirming it to be one of the Al-rich regions, and very little damage to the substrate was observed beneath the deposit in contrast to the extensively damaged surface in the absence of such a deposit, shown in Figure 8(a).

Although not shown, a similarly uniform but considerably thinner deposit was formed on the Al-13.5Mn specimen. This

difference in thickness of the deposit reflects the difference in cathodic currents for H_2O reduction on the two alloys. This, and the white colour of the deposit suggests it is $\text{Mg}(\text{OH})_2$ formed as a consequence of OH⁻ production at the cathodically polarized surface.

XRD spectra were recorded on Al-5.5Mn after cathodic polarization in both NaCl and MgCl_2 solutions, Figure 10. After polarization in NaCl, Al was shown to be present as $\text{Al}(\text{OH})_3$, Figure 10(a). A strong signal for Al was also observed, as expected, from the substrate alloy. No signal from the Al-Mn phases in the bulk material was observed in the spectrum. Figure 10(b) shows the XRD spectra recorded on Al-5.5Mn after potentiostatic polarization in the MgCl_2 solution. The peaks for $\text{Mg}(\text{OH})_2$ confirm the dominance of Mg identified in the XEDS spectrum in Figure 9(c). In addition, MnO_2 , Mn_2O_3 , $\text{Al}(\text{OH})_3$ and crystalline Al were also detected.

4 Discussion

The E_{CORR} values established on both Al-5.5Mn and Al-13.5Mn confirm they are considerably more noble, as expected, than the AZ31 matrix which has an E_{CORR} value of ~ -1.55 V which is typical of Mg alloys [29]. The E_{CORR} for Al-5.5Mn was unstable

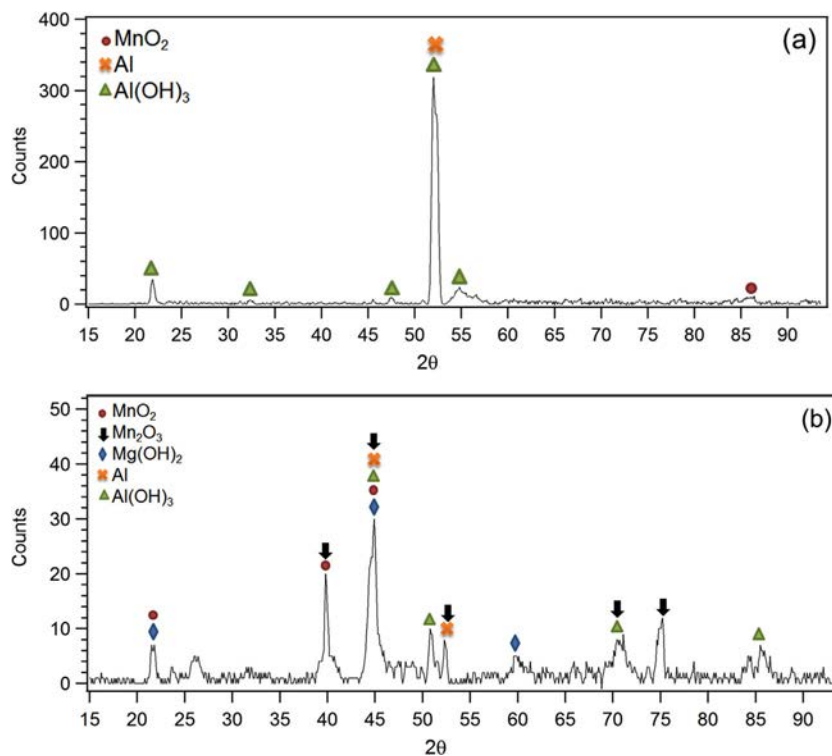


Figure 10. XRD spectra identifying the phases present on the Al-5.5Mn electrodes after cathodic polarization in (a) 0.275 M NaCl and (b) 0.138 M MgCl_2 solution.

over the first 3 h of exposure to 0.138 M MgCl_2 and throughout the 12 h exposure to 0.275 M NaCl. The potential transients suggest local metastable breakdown events, possibly associated with Mn-depleted Al-enriched regions of the alloy [30], which was observed recently on Al-Mn alloys [31]. Similar metastable events were not observed in E_{CORR} measurements on Al-13.5Mn. This increased stability of the Al-Mn alloy with an increased Mn content has previously been reported and attributed to the ability of Mn to improve the resistance to film breakdown due to a slight cathodic polarization of the Al matrix [9,32]. The eventual disappearance of these events on Al-5.5Mn in MgCl_2 compared to NaCl could be a consequence of the accumulation of small amounts of deposited $\text{Mg}(\text{OH})_2$. This would be consistent with the lower cathodic currents observed in the PDP scans (Figure 4) in the MgCl_2 solution compared to the NaCl solution at potentials only slightly negative to E_{CORR} . It is possible that the E_{CORR} established is dictated by the microgalvanic coupling between the Al-rich and Mn-rich areas of the surface, both alloys exhibiting a similar dual phase structure. Despite these transitory events the electrodes maintained their metallic appearance, (Figure 6(a) and (b)), after exposure at E_{CORR} confirming their (at least) short term stability. On polarization to -1.55 V any microgalvanic coupling would be overcome, and the major changes observed (Figure 6(c) and (d)) can be attributed to the instability of the alloys at the potential they would experience if microgalvanically coupled in a Mg alloy matrix.

The low cathodic current densities measured on Al-13.5Mn in both NaCl and MgCl_2 , Figure 5, suggest this alloy is a stable, but inefficient cathode. By contrast, the considerably higher

cathodic current densities measured on Al-5.5Mn suggest a more efficient but unstable cathode, especially in NaCl solution. The key difference between the two alloys is not their local composition but the relative fractions of the surface occupied by Al and Mn-enriched areas, suggesting that the high cathodic currents on Al-5.5Mn can be attributed to preferential H_2O reduction on the Al-rich areas. This would not be surprising since the exchange current density for H_2 evolution on Al ($\sim 10^{-8} \text{ A} \cdot \text{cm}^{-2}$) [33] is much greater than that on Mn ($\sim 10^{-11} \text{ A} \cdot \text{cm}^{-2}$) [34]. It is possible this difference could be larger since the reported exchange current value for Al was measured on the oxide-covered metal and the alloy may not have been passive at the pH conditions prevailing in the present experiment. This claim is consistent with previous studies which showed the cathodic reaction rate on an Al-Mn-Fe phase in a Mg alloy decreased as the Mn content increased [35]. This was attributed to the presence of a higher ratio of Mn:Fe in the phase. In a separate study, bulk additions of Mn (up to 2 wt %) were found to improve the corrosion resistance of a Mg-Zr system with a measured decrease in cathodic kinetics corresponding to the small additions of Mn [36]. In the present case the Al-Mn samples appeared free of contaminants, especially Fe, and the cathodic reactivity was decreased by an increase in Mn content. This is contrary to a previous report that Al-rich intermetallic particles will exhibit lower cathodic reactivity [10]. These results suggest that Al-Mn precipitates in the composition range $\text{Al}_{2.75}\text{Mn}$ ($\text{Al}_{11}\text{Mn}_4$) to $\text{Al}_{1.6}\text{Mn}$ (Al_8Mn_5) may only be particularly active cathodes within an α -Mg matrix if they are contaminated with impurities such as Fe.

The marked differences in cathodic current behaviour for Al-5.5Mn in NaCl and MgCl₂, Figure 5, reflect the suppression of H₂O reduction by the deposition of Mg(OH)₂ from the MgCl₂ solution. The rise in cathodic current density and erratic behaviour show this electrode was unstable under cathodic polarization in NaCl, while the lower steady cathodic current observed in MgCl₂ shows the presence of the Mg(OH)₂ deposit stabilized the alloy. That stabilization may not have been complete is suggested by the slow but noticeable increase in cathodic current in MgCl₂ over the 20 h duration of polarization, Figure 5.

The distinctly different surface features observed on Al-5.5Mn after cathodic polarization in the NaCl solution showed both heavily corroded and partially protected areas coexisted on the surface, Figures 7 and 8. The Al-rich substrate under the thicker surface deposit (Site 1, Figure 7, Sites 3 and 4 in the cross section in Figure 8(a)) was totally converted to corrosion product which XRD showed to be effectively Al(OH)₃. This extensive corrosion can be attributed to the generation of OH⁻ by H₂O reduction. After 20 h of polarization the bulk of the solution pH was 10.3 but is likely to be considerably higher since values as high as 14 can be achieved at this potential under microgalvanic coupling conditions in a Mg alloy [28]. Over this pH range, and at the applied potential of -1.55 V, Al is thermodynamically unstable in H₂O and unprotected by a passive oxide, and would be expected to corrode to yield soluble AlO₂⁻ [37] whose local precipitation would lead to the formation of the columnar, non-protective layer of Al(OH)₃ at Site 4. At the adjacent location on the Mn-rich area of the surface (Site 2 in Figure 7 and Site 5 in the cross section in Figure 8(a)) the substrate is more protected by a layer of Mn oxides/hydroxides containing a relatively small amount of Al(OH)₃. These observations are consistent with etching experiments on Al-Mn alloys in alkaline solutions [38] which show that corrosion proceeds via a preferential de-alloying process involving the loss by corrosion of Al to yield a Mn₃O₄ substrate surface layer. While these previous etching experiments were conducted at E_{CORR} (i.e., at a potential in the range -0.7 V to -1.0 V (Figure 3)) de-alloying of Al remains thermodynamically possible at -1.55 V.

These results show that one of the two phases more readily supports H₂O reduction at the expense of its own destruction (Al-rich phase) while the other (Mn-rich phase) is a less efficient cathode and partially protects itself by de-alloying to produce a predominantly Mn oxide/hydroxide layer. The formation of this last layer might be expected to further suppress H₂O reduction on the Mn-rich phase. This process coupled to the conversion of the Al-rich phase to the insulating Al(OH)₃ could account for the tendency of the cathodic current to slowly decrease with time as shown in Figure 5 (e.g., between 11 and 13 h). However, corrosion will progress through the Al-rich regions as indicated by the green arrows in Figure 8(a) while bypassing the Mn-rich locations. Such a location is outlined in red in Figure 8(a). This combination of features destabilizes the surface leading to the physical fractures observed and the exposure of previously buried Al-rich phase able to support H₂O reduction. This would account for the sudden increases in cathodic current observed (e.g., at ~13.5 h), Figure 8(a).

When Mg²⁺ was present in the solution, cathodic polarization led to the deposition of a thick surface layer of Mg(OH)₂ confirmed by XEDS (Figure 9(c)) and XRD measurements (Figure 10). This is not surprising given the solubility product for Mg(OH)₂ (K_{sp} = 1.8 × 10⁻¹¹) since its precipitation would be feasible for pH ≥ 9 [39]. At the electrode surface the local pH would be expected to be considerably higher (up to 14 [28]). The accumulation of this deposit would account for the very rapid decrease in cathodic current density on first applying cathodic polarization, Figure 5. The subsequent maintenance of a cathodic current density of ~100 μA · cm⁻² indicates that H₂O reduction continues probably at the base of the pores shown to be present in the FIB cross section (Figure 9(b)). This porosity would also explain the Al and Cl signals observed in the XEDS spectrum as these species would be able to diffuse through the porous Mg(OH)₂ deposit from solution (Figure 9(c)). The presence of Al (as Al(OH)₃) and Mn₂O₃/MnO₂ indicates some de-alloying of the substrate occurs under the alkaline conditions prevailing at that location. The relatively undamaged electrode/deposit interface (Figure 9(b)) compared to that after polarization in the absence of Mg²⁺ (Figure 8(a)) confirms the partial protectiveness of the Mg(OH)₂ deposit. The strong Cl signal can be attributed to the deposition of MgCl₂ within the pores when the electrode was removed from the cell and dried.

In a previous electron microscopy study of Al-Mn intermetallics on a corroded AM50 Mg alloy [20], three key observations were made: (1) domes of corrosion product comprised of MgO/Mg(OH)₂ deposited on the surfaces of Al-Mn intermetallic particles in the alloy; (2) fracture and delamination of the surfaces beneath the domes were accompanied by a depletion of Al on the surface, and (3) the collapse and apparent reconstruction of domes occurred on some Al-Mn intermetallics. The first two of these features have been reproduced on the Al-Mn materials used in this study when the alloy is polarized to the potential it would experience within an actively corroding Mg alloy.

While the results presented here demonstrate that Al-Mn phases, when present in Mg alloys, will act as cathodes for the reduction of H₂O (the key cathodic reaction) they also suggest that the rate will be controlled by a combination of chemical and physical features. The rate will be limited by the precipitation of a Mg(OH)₂ deposit due to the high pH generated by H₂ production and soluble Mg²⁺ transported to the cathode from adjacent anodic sites. The rate will be determined by the physical characteristics of this deposit, which was shown to be porous in this study allowing it to act as a partially protective permeable barrier. It is likely that the porosity, and hence the protectiveness, of the deposit is significantly over-estimated in the present study since the supply of soluble Mg²⁺ from the bulk of the solution could be much greater than that achievable by transport from the adjacent anodes in a corroding Mg alloy.

A second feature contributing to some control of H₂O reduction kinetics would be the instability of the Al-Mn substrate in the prevailing alkaline conditions. In this study this degradation process is likely to be exaggerated on the Al-5.5Mn alloy due to the coexistence of a large amount of the Al-rich phase which has a low Mn content and is not representative of the composition of the intermetallics in a Mg

alloy. In this regard the behavior observed on the Mn-rich phase ($\text{Al}_{2.75}\text{Mn}$ to $\text{Al}_{1.6}\text{Mn}$) is representative of what to expect in a Mg alloy. However, while the rate and extent of the de-alloying process may be different, the occurrence of this process has been demonstrated to occur both in this study and on Al_8Mn_5 particles in the AM50 Mg alloy [20].

The influence of this de-alloying process on the cathodic efficiency of microgalvanic coupling in Mg alloys remains difficult to quantify. While the accumulation of $\text{Mg}(\text{OH})_2$ and the creation of a Mn oxide/hydroxide surface by de-alloying would be expected to suppress H_2O reduction, the physical delamination of surface layers, as observed here and on the AM50 alloy, and the collapse of the domes of deposited $\text{Mg}(\text{OH})_2$ [20] would be expected to revive the reaction, at least temporarily.

Although not observed in this study, the domes of deposited $\text{Mg}(\text{OH})_2$ on particles in the AM50 alloy were sometimes observed to collapse and then regrow [20]. It is possible this could be caused by a combination of two effects. The demand for cathodic current on a rapidly corroding alloy would require a large current density on the small intermetallic particles and the consequent buildup of H_2 pressure within the pores in the dome could lead to its fracture and/or detachment. This would lead to a sudden surge in H_2 evolution on the freshly exposed Al-containing (and hence cathodically active) surface of the intermetallic. This sudden surge of current could assist the detachment of the dome and reinitiate the cycle leading to its reformation. Reformation of the corrosion product dome would then again slow cathodic activity, as observed on the Al-Mn electrodes in MgCl_2 .

As shown in Figure 1, an accumulation of corrosion product domes leading to a possible decrease in cathodic activity of the underlying Al-Mn features is important for the AZ31 alloy. Recently the propagation of corrosion on AZ31 in a filiform-like manner was attributed to the exposure of an increased number of cathodic sites as the corrosion front moved across the surface [40]. The initially exposed Al-Mn particles would sustain the cathodic reaction supporting the initial corrosion attack. However, as seen in Figure 1(d), as corrosion product domes accumulated on the particles, their ability to sustain H_2O reduction would be diminished. To sustain corrosion at a significant rate, one of two events would be necessary: 1) the collapse of the domes to reveal the intermetallic particle and regenerate its cathodic reactivity; 2) the exposure of new cathodically-active intermetallic particles in the already corroded areas. Since corrosion on AZ31 has been observed to propagate continuously despite suppression of cathodic reactivity by the accumulation of $\text{Mg}(\text{OH})_2$, it is likely that the exposure of new cathodes is required to sustain corrosion.

Some intermetallic particles have been shown not to accumulate corrosion product domes following corrosion under aqueous [9] and atmospheric conditions [41]. In these situations, the intermetallics are present within the eutectic α -phase, which has a higher Al-content than the α -Mg grains. Since these locations tend to passivate by the enrichment of Al near the oxide/alloy interface [9] they are isolated from the α -Mg grains and unable to microgalvanically couple. Clearly, the presence of a dome of accumulated corrosion product can be taken as an indicator of the cathodic activity of that particular intermetallic during corrosion of the Mg alloy.

5 Summary and conclusions

- Two Al-Mn alloys, Al-5.5Mn and Al-13.5Mn have been studied under both natural corrosion and cathodically polarized conditions in NaCl and MgCl_2 electrolytes.
- Since a primary goal of this study was to investigate the cathodic behaviour of Al-Mn intermetallic particles in Mg alloys, the composition and structure of the alloys were compared to that of the AZ31 alloy. The AZ31 alloy was found to contain particles with a composition ranging from $\text{Al}_{11}\text{Mn}_4$ to Al_8Mn_5 . The two Al-Mn alloys contained a phase with a similar composition but also an Al-rich phase containing only 3 to 5 at% Mn. The relative amount of this last phase was considerably higher in the Al-5.5Mn alloy.
- Over a 12h exposure period both alloys were stable experiencing only minor metastable pitting.
- When cathodically polarized to -1.55V in NaCl the Al-13.5Mn alloy supported only a small current for H_2O reduction and suffered only small amounts of de-alloying due to Al^{3+} release. By contrast, the Al-5.5Mn alloy sustained a large and increasing current for H_2O reduction and incurred extensive corrosion damage. This damage was primarily attributed to corrosion of the Al-rich phase in the alkaline conditions produced by the reduction of H_2O to H_2 . Delamination of the $\text{Al}(\text{OH})_3$ layer produced exposed Al-rich areas at deeper locations in the alloy allowing the cathodic current to steadily increase.
- When cathodically polarized in MgCl_2 the currents for H_2O reduction were significantly suppressed and the alloys protected against de-alloying/corrosion by the deposition of $\text{Mg}(\text{OH})_2$.

These results confirm that the accumulation of $\text{Mg}(\text{OH})_2$ and the corrosion/fracture/delamination observed on Al-Mn particles can be attributed to their function as microgalvanically coupled cathodes in Mg alloys.

Acknowledgements: This work was funded by a Collaborative Research and Development grant supported by NSERC and General Motors Canada. We would like to acknowledge the staff at Surface Science Western, Integrated Microscopy at the Biotron Research Institute, Nanofab and Professor *Roberta Flemming* from the Geology Department for their assistance with XRD measurements at Western University for their time and instrument use, *Janine Mauzeroll* and her group at McGill University, *Gianluigi Botton* and staff at the Canadian Centre for Electron Microscopy at McMaster University for the continuing collaboration in this project, and *Amjad Javaid* and the staff at CANMET Materials for materials acquisition.

6 References

- [1] B. L. Mordike, T. Ebert, *Materials Science and Engineering: A*, **2001**, 302, 37.
- [2] K. B. Deshpande, *Corrosion Science*, **2010**, 52, 2819.
- [3] H. Matsubara, Y. Ichige, K. Fujita, H. Nishiyama, K. Hodouchi, *Corrosion Science*, **2013**, 66, 203.

- [4] G. Song, A. Atrens, *Advanced Engineering Materials*, **2003**, 5, 837.
- [5] M. Taheri, J. R. Kish, N. Birbilis, M. Danaie, E. A. McNally, J. R. McDermid, *Electrochimica Acta*, **2014**, 116, 396.
- [6] J. A. Boyer, *American Magnesium Corporation 1927, Report No. 248*, 1–44.
- [7] R. E. McNulty, J. D. Hanawalt, *Transactions of The Electrochemical Society*, **1942**, 81, 423.
- [8] G. Ballerini, U. Bardi, R. Bignucolo, G. Ceraolo, *Corrosion Science*, **2005**, 47, 2173.
- [9] M. Zamin, *Corrosion*, **1981**, 37, 627.
- [10] R.-C. Zeng, J. Zhang, W.-J. Huang, W. Dietzel, K. U. Kainer, C. Blawert, W. Ke, *Transactions of Nonferrous Metals Society of China*, **2006**, 16, Supplement 2, s763.
- [11] A. Pardo, M. C. Merino, A. E. Coy, R. Arrabal, F. Viejo, E. Matykina, *Corrosion Science*, **2008**, 50, 823.
- [12] M. C. Merino, A. Pardo, R. Arrabal, S. Merino, P. Casajús, M. Mohedano, *Corrosion Science*, **2010**, 52, 1696.
- [13] S. Mathieu, C. Rapin, J. Steinmetz, P. Steinmetz, *Corrosion Science*, **2003**, 45, 2741.
- [14] R. M. Asmussen, W. J. Binns, P. Jakupi, D. Shoesmith, *Journal of The Electrochemical Society*, **2014**, 161, C501.
- [15] R. M. Asmussen, W. J. Binns, P. Jakupi, D. Shoesmith, *Corrosion*, **2014**, 71, 242.
- [16] M. Ascencio, M. Pegguleryuz, S. Omanovic, *Corrosion Science*, **2015**, 91, 297.
- [17] M. Ascencio, M. Pegguleryuz, S. Omanovic, *Corrosion Science*, **2014**, 87, 489.
- [18] S. V. Lamaka, O. V. Karavai, A. C. Bastos, M. L. Zheludkevich, M. G. S. Ferreira, *Electrochemistry Communications*, **2008**, 10, 259.
- [19] P. Dauphin-Ducharme, R. M. Asmussen, U. M. Tefashe, M. Danaie, W. J. Binns, P. Jakupi, G. A. Botton, D. W. Shoesmith, J. Mauzeroll, *Journal of The Electrochemical Society*, **2014**, 161, C557.
- [20] M. Danaie, R. M. Asmussen, P. Jakupi, D. W. Shoesmith, G. A. Botton, *Corrosion Science*, **2014**, 83, 299.
- [21] N. Birbilis, R. G. Buchheit, *Journal of The Electrochemical Society*, **2005**, 152, B140.
- [22] M. K. Cavanaugh, N. Birbilis, R. G. Buchheit, F. Bovard, *Scripta Materialia*, **2007**, 56, 995.
- [23] A. D. Südholz, N. T. Kirkland, R. G. Buchheit, N. Birbilis, *Electrochemical and Solid-State Letters*, **2011**, 14, C5.
- [24] N. Birbilis, R. G. Buchheit, *Journal of The Electrochemical Society*, **2008**, 155, C117.
- [25] K. Gusieva, C. H. J. Davies, J. R. Scully, N. Birbilis, *International Materials Reviews*, **2015**, 60, 169.
- [26] F. Andreatta, I. Apachitei, A. A. Kodentsov, J. Dzwonczyk, J. Duszczak, *Electrochimica Acta*, **2006**, 51, 3551.
- [27] P. Dauphin-Ducharme, R. M. Asmussen, D. W. Shoesmith, J. Mauzeroll, *Journal of Electroanalytical Chemistry*, **2015**, 736, 61.
- [28] J. Izquierdo, L. Nagy, I. Bitter, R. M. Souto, G. Nagy, *Electrochimica Acta*, **2013**, 87, 283.
- [29] T. Cain, L. G. Bland, N. Birbilis, J. R. Scully, *Corrosion*, **2014**, 70, 1043.
- [30] T. P. Moffat, G. R. Stafford, D. E. Hall, *Journal of The Electrochemical Society*, **1993**, 140, 2779.
- [31] B. Wang, J. Liu, M. Yin, Y. Xiao, X. H. Wang, J. X. He, *Materials and Corrosion*, **2016**, 67, 51.
- [32] Z. Szklarska-Smialowska, *Corrosion Science*, **1999**, 41, 1743.
- [33] A. K. Vijh, *The Journal of Physical Chemistry*, **1969**, 73, 506.
- [34] A. Bélanger, A. K. Vijh, *Journal of The Electrochemical Society*, **1974**, 121, 225.
- [35] O. Lunder, T. K. Aune, K. Nisancioglu, *Corrosion*, **1987**, 43, 291.
- [36] D. S. Gandel, M. A. Easton, M. A. Gibson, N. Birbilis, *Corrosion*, **2013**, 69, 744.
- [37] P. Marcel, M. Pourbaix, *Atlas of Electrochemical Equilibria in Aqueous Solutions*, 2d English ed., National Association of Corrosion Engineers, Houston, TX **1974**.
- [38] C. Xu, R. Wang, Y. Zhang, Y. Ding, *Nanoscale*, **2010**, 2, 906.
- [39] Haynes, W. M., *CRC handbook of chemistry and physics*. CRC press, Boca Raton **2013**.
- [40] G. Williams, H. Llwyd Dafydd, R. Grace, *Electrochimica Acta*, **2013**, 109, 489.
- [41] M. Jönsson, D. Persson, R. Gubner, *Journal of The Electrochemical Society*, **2007**, 154, C684.

(Received: March 15, 2015)

W8349

(Accepted: April 7, 2015)